Unsteady Laminar Natural Convection, Radiation and Conduction within an Enclosure with an Obstruction

M. Faghri, Y. Asako, G. M. Berard and A. Chaboki[1]

A numerical unsteady two-dimensional heat transfer and fluid flow analysis has been conducted on a square enclosure with a centered square obstruction. The analysis includes conduction, laminar natural convection and radiation with a radiatively non-participating fluid. Uniform temperature boundary-conditions are prescribed on the left and right enclosure surfaces, whereas the top and bottom surfaces are maintained at an adiabatic condition. Non-dimensionalized governing equations are solved using a control volume finite difference scheme coupled to a radiation algorithm. The calculations are performed for three enclosure lengths ($L = 0.025\,\text{m}, 0.050\,\text{m}, 0.100\,\text{m}$), for six maximum enclosure temperature differences ($\Delta T = 20°, 50°, 100°, 200°, 300°, 400°\,\text{K}$) and for two thermal diffusivity ratios ($\alpha^* = 0.115, 2.902$). Results are displayed in the form of streamline and isotherm plots, velocity and radiation heat flux plots and tabulated radiation and convective Nusselt numbers. They are also compared with recent literature in radiation and convection within enclosures.

INTRODUCTION

High temperature heating and cooling within enclosures exists in many practical applications, such as fire prevention, electronic cooling and heat treatment of materials. In these applications, the mechanisms of heat transfer are natural convection and radiation. As indicated by Ostrach [1], a multitude of research has been accomplished for natural convection within rectangular and cylindrical enclosures. Kübleck et al. [2] has completed numerical predictions of unsteady numerical laminar natural convection within a square enclosure while House et al. [3], considered steady laminar natural convection within a square enclosure with a centered obstruction. Steady state results were compared with House in Berard [4].

Research in combined laminar natural convection, conduction and radiation in enclosures has been investigated by Larson and Viskanta [5], Chang et al. [6], Nakamura et al. [7] and Chaboki et al. [8]. Larson and Viskanta considered unsteady heat transfer in a square enclosure while Chang included a steady analysis with two vertical fins. Nakamura considered two rectangular enclosures separated by a vertical partition. Chaboki compared actual test results to numerical unsteady natural convection and radiation results within an enclosure with a circular obstruction. As can be seen, all the previous analyses, with the exception of Larson and Viskanta and Chaboki, considered steady to simple enclosure geometries. This motivated the solutions for unsteady combined natural convection, radiation and conduction to enclosures with complex internal geometries, as in a thesis by Berard [4], where a simple square obstruction is addressed.

The numerical methodology developed in this study utilizes the control volume finite differencing scheme coupled with a radiation

1. Department of Mechanical Engineering, The University of Rhode Island, Kingston, RI 02881, U.S.A.
Scientia Iranica, Vol. 1, No. 1, © Sharif University of Technology, April 1994.

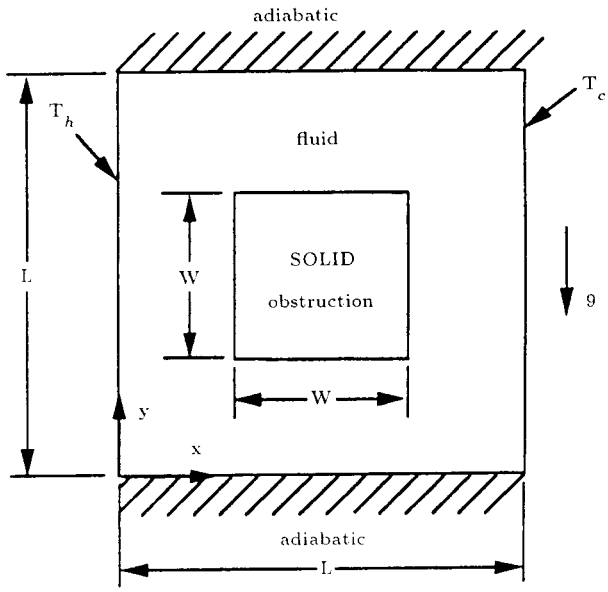

Figure 1. Diagram of enclosure with obstruction.

algorithm. Buoyancy is predicted via the Boussinesq approximation. Numerical solutions are obtained for three enclosure lengths ($L = 0.025$ m, 0.050 m, 0.100 m), six maximum enclosure temperature differences ($\Delta T = 20°, 50°, 100°$, 200°, 300°, 400° K), and two thermal diffusivity ratios ($\alpha^* = 0.115$, 2.902). Results are displayed in the form of streamline and temperature contour plots and, tabulated radiation and convective Nusselt numbers. Results are compared to a combined radiation/convection numerical study by Nakamura et al. [7]. Other comparisons with limiting cases are documented by Berard [4].

FORMULATION

The problem to be considered in this study consists of a square enclosure of length L, and a square obstruction of length W which is located in the center of the enclosure as shown in Figure 1. The left wall of the enclosure is at a constant temperature T_h and the right is at a constant temperature T_c. Top and bottom walls are adiabatic. The entrained fluid is considered to be radiatively non-participating and the flow assumed to be laminar.

The following parameters are introduced to non-dimensionalize the governing equations:

$$U = uL/\alpha_f;$$

$$V = vL/\alpha_f;$$

$$X = x/L;$$

$$Y = y/L;$$

$$\tau = t\alpha_f/L^2;$$

$$\theta = (T - T_c)/(T_h - T_c). \tag{1}$$

Variations in density are assumed to be negligible in the continuity, momentum and energy equations, except for the buoyancy term in the y-momentum equation (Boussinesq approximation). This leads to the following conservation equations for continuity, x- and y-momentum equations and energy equations for the fluid and the solid.

$$\frac{\partial U}{\partial X} + \frac{\partial V}{\partial Y} = 0, \tag{2}$$

$$\frac{\partial U}{\partial \tau} + U\frac{\partial U}{\partial X} + V\frac{\partial U}{\partial Y} = Pr\left[\frac{\partial^2 U}{\partial X^2} + \frac{\partial^2 U}{\partial Y^2}\right] - \frac{\partial P^*}{\partial X}, \tag{3}$$

$$\frac{\partial V}{\partial \tau} + U\frac{\partial V}{\partial X} + V\frac{\partial V}{\partial Y} = Pr\left[\frac{\partial^2 V}{\partial X^2} + \frac{\partial^2 V}{\partial Y^2}\right] - \frac{\partial P^*}{\partial Y} + RaPr\theta, \tag{4}$$

$$\frac{\partial \theta}{\partial \tau} + U\frac{\partial \theta}{\partial X} + V\frac{\partial \theta}{\partial Y} = \left[\frac{\partial^2 \theta}{\partial X^2} + \frac{\partial^2 \theta}{\partial Y^2}\right], \tag{5}$$

$$\frac{\partial \theta}{\partial \tau} = \alpha^*\left[\frac{\partial^2 \theta}{\partial X^2} + \frac{\partial^2 \theta}{\partial Y^2}\right], \tag{6}$$

where $P^* = (P + \rho_o gY)L^2/\rho_o\alpha_f^2$,
$Ra = g\beta L^3(T_h - T_c)/\alpha\nu$, and $Pr = \nu/\alpha$.

Boundary Conditions

Boundary conditions include a no-slip condition at the solid surfaces for the momentum equations. For the energy equation, constant hot and

cold wall temperatures are assigned to the left and right walls of the enclosure respectively, as shown in Figure 1, and top and bottom walls are insulated. The emissivity ratio, ε^*, between the solid surfaces is assumed to be equal to one. Internal fluid and obstruction are initially at a specified uniform temperature. The internal fluid is initially at rest with $U_i = 0$: The above boundary conditions are summarized below:

$$\left.\begin{aligned} &\theta(X,Y) = 0 \text{ for } \tau < 0 \text{ and,} \\ &\theta(0,Y) = 1; \quad \theta(1,Y) = 0 \\ &\frac{\partial\theta(X,1)}{\partial Y} - N_r Q_r\Big|_{Y=1} = 0 \\ &\frac{\partial\theta(X,0)}{\partial Y} - N_r Q_r\Big|_{Y=0} = 0 \end{aligned}\right\} \text{ for } \tau \geq 0. \qquad (7)$$

Where N_r is the radiation/conduction number and is equal to $\sigma T_h^4 L/k_f \Delta T$, σ is the Stephan-Boltzman constant, and ΔT is the maximum temperature difference in the enclosure, $T_h - T_c$. Q_r is the non-dimensionalized thermal radiation or radiosity from the other surfaces and is equal to $q_r/\sigma T_h^4$. This quantity is determined from a radiation analysis that is described now.

Internal Radiation Heat Transfer

Radiation exchange within an enclosure with gray diffuse surfaces and an arbitrary surface temperature distribution is given by the following equation:

$$\sum_{i=1}^{m} Gi = \sum_{i=1}^{m}(\varepsilon_i \sigma T_i^4 + (1-\varepsilon_i)\sum_{j=1}^{m} J_j), \qquad (8)$$

where G_i is the radiosity which is the net radiation energy leaving the heated ith. The first term on the right of Equation 8 is the radiant energy being emitted by surface i. The second term on the right hand side of the equation is the reflected radiant energy from surrounding surfaces that can be 'seen' by surface i. J_j is the incident radiation from the surrounding surfaces. For an arbitrary surface:

$$J_j = \int_{\eta=0}^{\eta=L} G_j(\eta)\frac{dF_{\delta j\to\delta i}}{d\eta}d\eta, \qquad (9)$$

where $F_{\delta j\to\delta i}$ is what is commonly known as the shape factor from a differential surface δj to δi along some arbitrary length η. A detailed derivation is summarized in Berard [4].

Calculation of shape factors is accomplished via the cross-string method and the line-line-cross technique. The cross-line method is summarized in Hottel and Sarofim [9] and is used to calculate the shape factor between perpendicular and parallel two-dimensional surfaces. The line-line-cross technique is a hidden line algorithm used to determine the presence of an obstruction between two radiation surfaces. This technique is summarized in Berard [4].

The net heat flux on a surface may be shown as:

$$q_r = G_i - \sum_{\substack{j=1 \\ j\neq i}}^{m}(F_{j\to i})(G_j). \qquad (10)$$

Numerical Solutions

The discretized procedure of the conservation equations was based on the control volume finite difference scheme. Using the power-law profile, the discretized equations are solved by using the line-by-line method. The matrix method was utilized in the solution of surface radiation heat fluxes.

Supplementary calculations for $L = 0.100$ m, $Ar = 0.5$, $\varepsilon^* = 1.0$, $\alpha^* = 2.902$ and $\Delta T = 400°$ K were performed with (20×20), (40×40), and (100×100) grid points to determine the accuracy of the model. Grids in the fluid region between the vertical walls and the obstruction were non-uniform with denser grids near the hot and cold

Table 1. Grid Size Effect on Nu, Nur, and Elapsed Time

Grid	Nu	Nur	Elapsed Time
20 × 20	11.28	26.86	0.02710
40 × 40	7.64	27.78	0.03898
100 × 100	7.61	27.57	0.04089

walls. Uniform grids were used in the obstruction. Results of this study are summarized in Table 1.

As seen from this table, the percent difference in the average steady state Nusselt between the medium mesh (40 × 40) and the coarse mesh (20 × 20) is 47.6%. The percent difference in the average steady state Nusselt between the medium mesh and the fine mesh (100 × 100) is −0.39%. The difference in the radiation average steady state Nusselt number, Nur, is −33.1% between the medium mesh and the coarse mesh and −0.75% between the medium mesh and fine mesh. Finally, total elapsed time differences between the medium mesh and the coarse and fine mesh is −30.48% and 4.9% respectively. Thus, use of a medium mesh yields accurate results and minimizes computer costs.

A timestep of 1.0×10^{-5} was used in all analyses. Three timesteps were investigated, $1.0 \times 10^{-4}, 1.0 \times 10^{-5}$ and 1.0×10^{-6}. Using the same parameters as in the grid study with a medium mesh, the last two timesteps converged to the same Nusselt number results. The initial timestep, 1.0×10^{-4}, became unstable and oscillated about an average point. Therefore, a 1.0×10^{-5} timestep was used until a steady state condition was achieved. Steady state was achieved once the difference between the left wall and the right wall heat fluxes was less than 1% of the total left wall heat flux.

The algorithm is compared to the results derived from Nakamura et al. [7]. A rectangular enclosure bisected by a thin partition geometry

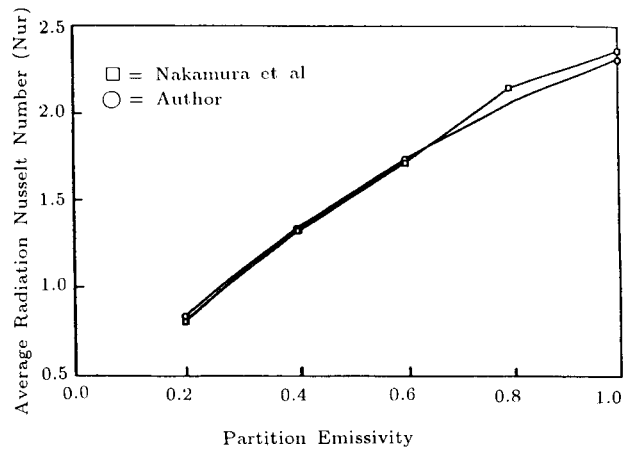

Figure 2. Comparison to Nakamura et al.

with top, vertical and partition emissivities, $\varepsilon_T, \varepsilon_H$, and ε_P respectively, were modeled. In this analysis, $\varepsilon_H = 0.5$ and $\varepsilon_T = 0.03$ for ε_P equal to $0.2, 0.4, 0.6, 0.8$ and 1.0 . The average radiation Nusselt number, Nur, for the hot wall was calculated and plotted on Figure 2 as a comparison to Nakamura's results. The results demonstrate excellent correlation with Nakamura's results. Other comparisons were accomplished with House et al. [3] and De Vahl Davis [10]. These results are summarized in Berard [4].

The computations were executed on the CRAY YMP supercomputer located at the Pittsburgh Supercomputing Center through a federally funded national grant. A typical execution time on the CRAY supercomputer was approximately $2\frac{1}{2}$ hours.

The analysis applies three enclosure lengths of 0.025 m, 0.05 m and 0.10 m. Hot and cold wall temperatures were 693° and 293° K, respectively. The fluid chosen was dry air with the thermophysical properties evaluated at the mean temperature; $k_f = 0.0405$ W/m−° K, $g\beta/\nu^2 = 0.1081 \times 10^8$ 1/° K− m^3, Pr = 0.72, and $\alpha = 33.6 \times 10^{-6}$ m^2/s. The Rayleigh and radiation/conduction numbers are calculated as a function of the enclosure length L as follows:

$$Ra = \left[\frac{g\beta}{\nu^2}\right][Pr][L^3][\Delta T], \tag{11}$$

$$Nr = \frac{\sigma T_h^4 L}{K_f \Delta T}. \tag{12}$$

Thermal diffusivities of the obstruction are chosen such that a high and low α^* is obtained. Two materials commonly subjected to high temperature heat treatments or environmental conditions were chosen. These are 302 stainless steel and aluminum 6061 – T6. The diffusivities and their ratios are listed in Table 2.

A listing of all cases computed is listed in Table 3. Cases 1 through 3 relate to an enclosure length of 0.025 m through 0.100 m, respectively, at $\alpha^* = 0.115$. Cases 4 through 6 are similar to cases 1 through 3 with the exception that $\alpha^* = 2.902$. The remaining cases were used to investigate the effect of the maximum temperature difference, ΔT, with the enclosure.

Nusselt Numbers

The average convective Nusselt number may be interpreted as the temperature slope near the wall:

$$Nu = \frac{hL}{k} = \sum_{i=1}^{m} \frac{\Delta\theta}{\Delta X} \Delta Y_i \Big|_{X=0}, \tag{13}$$

The radiation Nusselt number compares the total energy input to a surface compared to the total energy emitted.

$$Nu_r = \sum_{i=1}^{m} Q_{r_i} N_r \Delta Y_i |_{X=0}. \tag{14}$$

Table 2. Material Properties Used in Calculations

Material	α	α^*
302 Stainless Steel	3.87×10^{-6} m^2/s	0.115
Aluminum 6061 – T6	97.5×10^{-6} m^2/s	2.902

Table 3. Listing of Parametric Cases

Case No.	L	Ra	Nr	σ^*	Ar	α^*	ΔT
1	0.025	4.80E04	20.18	0.115	0.50	1.0	400
2	0.050	3.84E05	40.36	0.115	0.50	1.0	400
3	0.100	3.07E06	80.72	0.115	0.50	1.0	400
4	0.025	4.80E04	20.18	2.902	0.50	1.0	400
5	0.050	3.84E05	40.36	2.902	0.50	1.0	400
6	0.100	3.07E06	80.72	2.902	0.50	1.0	400
7	0.100	5.46E06	66.58	0.115	0.50	1.0	300
8	0.100	5.83E06	52.33	0.115	0.50	1.0	200
9	0.100	4.91E06	47.29	0.115	0.50	1.0	100
10	0.100	3.38E06	58.35	0.115	0.50	1.0	50
11	0.100	1.68E06	105.47	0.115	0.50	1.0	20

RESULTS AND DISCUSSION

Streamline, isotherm contour plots, V-velocity and hot wall heat flux plots for the two different cases are displayed in Figures 3 through 5. As can be seen from Table 4, which shows comparison of results with respect to convection and radiation Nusselt numbers. In these three cases, the thermal diffusivity ratio, α^*, and the hot

Table 4. Comparison of Results for Nusselt Numbers

Case No.	Nu	% of Total	Nur	% of Total
1	2.32	26.5%	6.43	73.5%
2	4.47	26.5%	12.40	73.5%
3	8.04	25.4%	23.63	74.6%
4	2.02	20.5%	7.82	79.5%
5	4.21	21.9%	14.98	78.1%
6	7.64	21.6%	27.78	78.4%
7	10.13	33.9%	19.79	66.1%
8	11.08	42.4%	15.04	57.6%
9	11.38	51.0%	10.92	49.0%
10	10.64	54.1%	9.03	45.9%
11	8.94	53.1%	7.89	46.9%

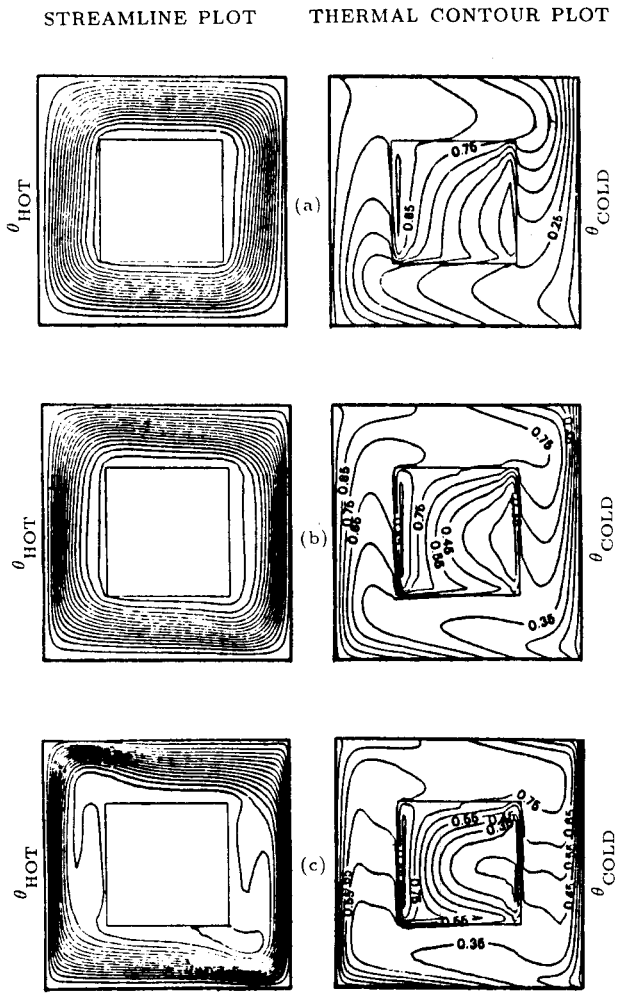

Figure 3. Steady state streamline and thermal contour plots.

and cold wall temperatures, T_h and T_c, are held constant while the enclosure length, L, is varied. The effect of changes in the overall enclosure length is reflected in the Rayleigh number, Ra, and the radiation/conduction number, Nr.

Steady state streamline and isotherm plots may be seen in Figure 3 for cases 1, 2 and 3, and associated enclosure lengths 0.025 m, 0.050 m and 0.100 m, respectively, where

$Pr = 0.72$,
$\alpha^* = 0.115$,
$\epsilon = 1.0$,
$Ar = 0.5$ and

(a) $L = 0.025$ m,
(b) $L = 0.050$ m,
(c) $L = 0.100$ m.

Figure 3 differs significantly from what would be expected from a convection alone solution. In convection alone solutions, such as from House et al. [3], as the Rayleigh number increases, the upper wall temperature is almost constant except near the upper right hand side of the enclosure where there is a large gradient. This is the effect of the hot fluid heating up the upper enclosure wall. The same effect is seen on the cold side of House's enclosure, where fluid being cooled by the cold wall cools off the lower portion of the enclosure wall. There is again a large temperature gradient, as one would expect on the lower left hand side of the enclosure.

Heat from the left side of the enclosure radiates outwardly to heat both the upper and lower walls. Alternately, the cold wall cools the upper and lower walls via radiation as a radiant heat sink. The net effect is that the warmer isotherms for any Rayleigh number has a much less reaching effect on the upper wall and a much more reaching effect on the lower wall. In effect, the lower wall of the enclosure is heating up the fluid more significantly than with convection alone. On the top wall, the fluid is warmer than the surrounding enclosure walls, therefore, the fluid is being cooled more significantly than is seen in convection alone. In cases of convection alone, isotherm lines vary from vertical lines at low Rayleigh numbers and diagonal lines from the upper right corner of the enclosure to the lower left corner of the enclosure for higher Rayleigh numbers.

In Figure 3c, the streamline flow differs from the lower Rayleigh number cases, 1 and 2 (Figures 3a and 3b , respectively). Secondary circulation patterns have developed in the steady state solution of case 3, Figure 3c. The results indicate a secondary circulation pattern in the upper left hand region of the enclosure and, also, a secondary circulation pattern near the lower

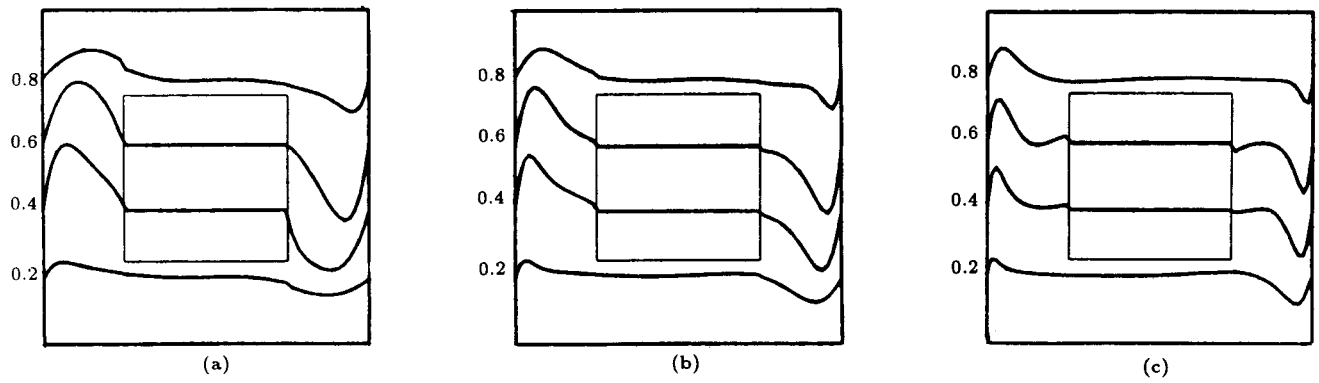

Figure 4. V-velocity plots.

right region of the enclosure.

The obstruction hot surface creates another thermal boundary layer on the obstruction wall. This becomes very evident in Figure 4*c*, the V-velocity plot, where $Y = 0.2, 0.4$, 0.6 and 0.8 for

$Pr = 0.72$,

$\alpha^* = 0.115$,

$\varepsilon^* = 1.0$,

$Ar = 0.5$ and

(a) $L = 0.025\,\text{m}$,

(b) $L = 0.050\,\text{m}$,

(c) $L = 0.100\,\text{m}$.

In this plot, a boundary layer developing on the enclosure hot and cold walls can be seen. A similar, but not as prevalent, boundary layer developing on the obstruction vertical walls can also be visualized.

The natural convection boundary layer within the gap is driven by the temperature gradient in this area. It can be seen in Figure 3a, that the temperature gradients near the enclosure hot and cold walls are fairly evenly distributed. Referring to Figure 4a, this causes a maximum vertical velocity slightly off center of the gap near the hot wall and a minimum vertical velocity near the cold. For slightly higher Rayleigh and radiation/conduction numbers the vertical velocity is skewed more toward the hot and cold wall surfaces. In Figure 3b, since there is a greater temperature gradient near the hot and cold wall, the velocity appears to be much closer to these surfaces. Also, since the opposing obstruction surface is hotter than the previous case, the beginnings of another boundary layer may be seen in Figure 4b.

In Figure 4c, the higher velocity is very much near the hot and cold walls where there exists a very steep thermal gradient. The flow in the center of the gaps is essentially zero and there is a greater hint of a secondary boundary layer on the obstruction surfaces.

Figure. 5 displays the normalized heat flux along the hot wall. In this plot,

$Pr = 0.72$,

$\alpha^* = 0.115$,

$\varepsilon^* = 1.0$,

$Ar = 0.5$ and,

(a) $L = 0.025\,\text{m}$,

(b) $L = 0.050\,\text{m}$,

(c) $L = 0.100\,\text{m}$.

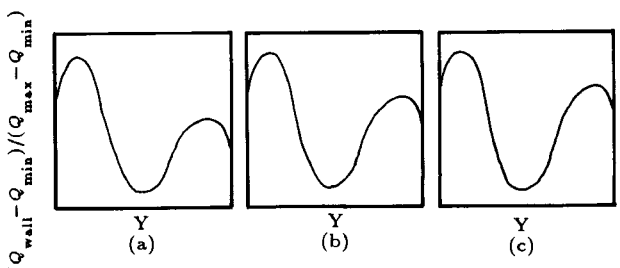

Figure 5. Hot wall radiation heat flux plots.

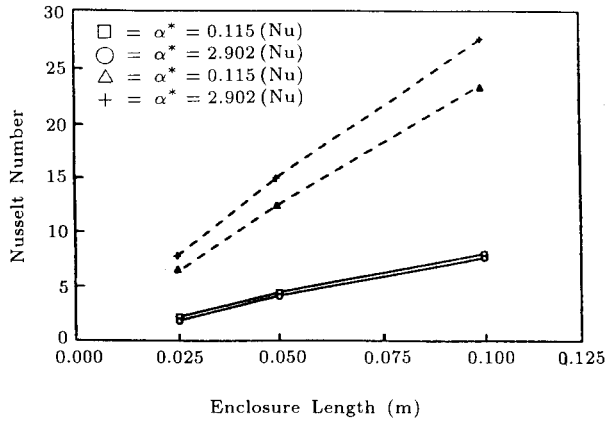

Figure 6. Total Nusselt number versus enclosure length.

The local heat flux is normalized by scanning the heat flux along the entire length of the wall and locating the minimum and maximum heat flux.

The effect of a low diffusivity ratio, α^*, is reflected in the thermal contours within the obstruction. Isotherms in the center of the obstruction are almost vertical and bend depending on the exterior flow and the radiation heat flux. The core appears to maintain its temperature regardless of the exterior conditions. Near the exterior walls however, thermal gradients are extremely large as local areas are heated up or cooled down. With a low diffusivity, penetration of surface heat fluxes into the obstruction is hindered.

The effect of the increase in enclosure length and the corresponding increases in the Rayleigh number and radiation/conduction number is summarized in the Nusselt number results. As the enclosure length increases, both convection and radiation Nusselt numbers increase proportionately as displayed in Figure 6. The ratio of the measure of convective heat transfer to the total heat transfer by radiation and convection remains the same at approximately 0.26 for all cases.

Elapsed Time Study

The flow patterns at several different times were stored and plotted in order to observe the flow and thermal patterns as they developed. Transient solutions for case 6 are shown in Figure 7, where

$Pr = 0.72,$
$\alpha^* = 0.115,$
$\varepsilon^* = 1.0,$
$Ar = 0.5$ and
$L = 0.100$ m.

Plots range from the early onsets of the flow until just before achieving steady state. The non-dimensionalized times, τ , are (a) 0.001, (b) 0.002, (c) 0.0025, (d) 0.003, (e) 0.010, and (f) 0.020.

As displayed in Figure 7, it would appear that two separate secondary circulation patterns have appeared in the streamline plot. One in the upper left corner of the enclosure, and an elongated one on the left vertical surface of the obstruction.

Isopleths in the thermal contour plot suggest that the fluid near the hot wall of the enclosure and along the bottom and top walls are achieving a temperature much higher than the surrounding fluid. This verifies Larson and Viskantas observation [5]. Larson and Viskanta noted that in a square enclosure when radiation and convection are considered, the cold wall facing the hot wall rapidly heats up even before the fluid temperature begins to convect the heat to the other surfaces. This effect appears to be almost instantaneous. Due to the high thermal diffusivity of the obstruction to that of the fluid, the temperature field has quickly permeated into the obstruction.

CONCLUSIONS

A parametric unsteady numerical analysis has been conducted on a square enclosure with a centered square obstruction. The analysis included conduction, natural convection and radiation with a radiatively non-participating fluid.

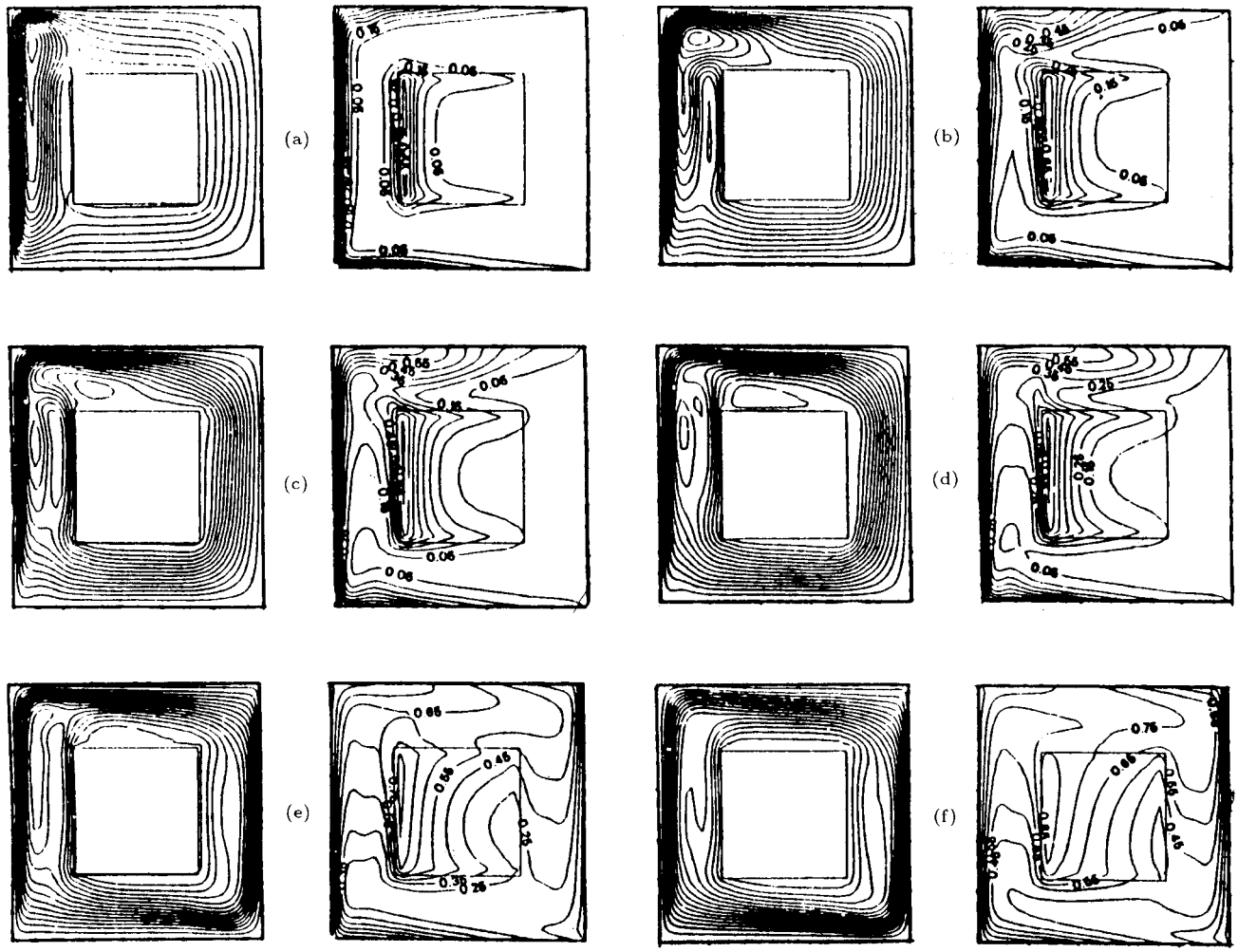

Figure 7. Streamline and thermal contour plots.

Isotherm and streamline results demonstrate a significant difference with the addition of radiation into the solution. Fluid in the enclosure-obstruction gap is heated (or cooled) more significantly due to the radiation heating (cooling) of the obstruction wall from the enclosure wall. This is evident from the formation of the boundary layer on the obstruction surface.

The effect of enclosure length on the total average Nusselt number appears to be linear. Doubling the enclosure length and maintaining the aspect ratio doubles the average Nusselt number regardless of the thermal diffusivity ratio. Further results with aspect ratios, thermal diffusivity ratios, and emissivity ratios are summarized in Berard [4].

The time to reach steady state conditions is accelerated for high thermal diffusivity ratios and hindered with low ratios. From observations it would seem that the ideal case, when considering time, is a large enclosure, i.e., large Rayleigh number and radiation/conduction number, high thermal diffusivity ratio and large aspect ratio. The larger the enclosure, the more heat flux is being input into the system. The least ideal case would be a small enclosure, low thermal diffusivity ratio and large aspect ratio.

NOMENCLATURE

Ar	aspect ratio, W/L
c	specific heat

$F_{i\to j}$	shape factor from surface i to surface j
G	radiosity
g	acceleration due to gravity
h	heat transfer coefficient
J_i	incident radiation from surface i
k	thermal conductivity
L	enclosure length
m	number of radiation surfaces
Nr	radiation/conduction number, $\sigma T_h^4 L/k_f \Delta T$
Nu	convective Nusselt number
Nu_r	radiation Nusselt number
P	pressure
P^*	non-dimensional pressure, $(P+\rho_o g y)L^2/\rho_o \alpha_f^2$
Pr	Prandtl number, ν/α
Q_r	non-dimensionalized thermal radiation, $q_r/\sigma T_h^4$
q_r	radiation heat flux
Ra	Rayleigh number, $g\beta(T_h - T_c)L^3/\nu\alpha$
T	temperature
t	time
U	non-dimensionalized u-velocity, uL/α_f
u	fluid velocity in x direction
V	non-dimensionalized v-velocity, vL/α_f
v	fluid velocity in y direction
W	obstruction width (m)
X	non-dimensionalized length, x/L
x	length along x-axis
Y	length along y-axis
y	non-dimensionalized length, y/L
α	thermal diffusivity
α^*	thermal diffusivity ratio, α_{obs}/α_f
β	coefficient of thermal expansion
ΔT	hot and cold wall temperature difference, $T_h - T_c$
ε	emissivity
ε^*	emissivity ratio, $\varepsilon_{wall}/\varepsilon_{obs}$
θ	non-dimensionalized temperature, $(T_n - T_c)/(T_h - T_c)$
υ	kinematic viscosity
η	length variable
ρ	density
σ	Stephan-Boltzman constant, $5.67 \times 10^{-8}\,\mathrm{W/m^2-K^4}$
τ	non-dimensionalized time, $t\alpha_f/L^2$

Subscripts

$c/COLD$	cold wall
f	fluid
h/HOT	hot wall
i,j	indices
o	reference
obs	obstruction
r	radiation
s	steady state
$wall$	pertaining to enclosure wall
x	x direction
y	y direction

REFERENCES

1. Ostrach, S. and Austin, W. "Natural convection in enclosures," *J. of Heat Transfer*, **110**, pp 1175-1190 (1988).
2. Kübleck, K., Merker, G. P. and Straub, J. "Advanced numerical computation of two-dimensional time-dependent free convection in cavities," *Int. J. of Heat Mass Transfer*, **23**, pp 203-217 (1980).
3. House, J. M., Beckerman, C. and Smith, T. F. "Natural convection heat transfer in a

square enclosure containing an obstruction," *Heat Transfer in Convective Flows,* 1988 National Heat Transfer Conference HTD-107 (1989).

4. Berard, G. M. "Unsteady laminar natural convection, radiation and conduction within an enclosure with an obstruction," Master of science thesis, University of Rhode Island, USA (1991).
5. Larson, D. W. and Viskanta, R. "Transient combined laminar free convection and radiation in a rectangular enclosure," *J. of Fluid Mechanics*, **78**, part 1, pp 65-85 (1976).
6. Chang, L. C., Yang, K. T. and Lloyd, J. R. "Radiation-natural convection interactions in two-dimensional complex enclosures," *J. of Heat Transfer,* **105**, pp 89-95 (1983).
7. Nakamura, H., Asako, Y. and Hirata, H. "Combined free convection and radiation heat transfer in rectangular cavities with a wall partition," *Transactions of the JSME*, **50** (459B), pp 2647-2654 (1984).
8. Chaboki, A., Langlie, S., Kneer, M., Faghri, M. and Berard, G. "A numerical prediction method for fast cook-off of rocket motors contained inside launch canisters," JANNAF Propulsion Systems Hazard Subcommittee Meeting (1990).
9. Hottel, H. C. and Sarofim, A. F. *Radiative Transfer*, McGraw-Hill Book Co., New York, USA, pp 31-39 (1967).
10. De Vahl Davis, G. "Natural convection of air in an square cavity: A benchmark numerical solution," *Int. J. of Numerical Methods in Heat Transfer,* **3**, pp 249-264 (1983).